Control of bursting synchronization in networks of Hodgkin-Huxley-type neurons with chemical synapses

C. A. S. Batista,[1] R. L. Viana,[1,*] F. A. S. Ferrari,[1] S. R. Lopes,[1] A. M. Batista,[2] and J. C. P. Coninck[1]

[1]*Departament of Physics, Federal University of Paraná, Curitiba, Paraná, Brazil*
[2]*Departament of Mathematics and Statistics, State University of Ponta Grossa, Ponta Grossa, Paraná, Brazil*

Thermally sensitive neurons present bursting activity for certain temperature ranges, characterized by fast repetitive spiking of action potential followed by a short quiescent period. Synchronization of bursting activity is possible in networks of coupled neurons, and it is sometimes an undesirable feature. Control procedures can suppress totally or partially this collective behavior, with potential applications in deep-brain stimulation techniques. We investigate the control of bursting synchronization in small-world networks of Hodgkin-Huxley-type thermally sensitive neurons with chemical synapses through two different strategies. One is the application of an external time-periodic electrical signal and another consists of a time-delayed feedback signal. We consider the effectiveness of both strategies in terms of protocols of applications suitable to be applied by pacemakers.

PACS number(s): 87.19.lg, 87.19.lj, 87.18.Sn

I. INTRODUCTION

The brain consists of about 100 specialized modules with different functions, each of them a complex network itself, and is thus a paradigmatic example of a complex dynamical system [1]. The network unit, the neuron, receives excitatory inputs from a few thousands of other neurons and processes them according to some deterministic rules [2]. Models of biological neuronal networks must consider both the intrinsic dynamics at each neuron as well as their connection architecture [3]. Moreover, there are both electrical (gap-junction) and chemical synapses, the latter being excitatory or inhibitory and possessing a dynamics of their own depending on the neuron behavior. The synaptic connectivity is dynamically altered by changes in strength as a response to either use or disuse of transmission over the synapse itself and also by changes in the quantity and absorption properties of neurotransmitters [4]. Such mechanisms of synaptic plasticity are key factors explaining such high-level brain activities as memories and learning.

A dynamical description of a bursting neuron requires the use of mathematical models possessing two time scales: (i) a fast time scale characterized by repetitive spiking and (ii) a slow time scale with bursting activity, where neuron activity alternates between a quiescent state and spiking trains [5]. The spiking dynamics of the action potentials can be described by the Hodgkin-Huxley model, which is a conductance-based model of an excitable neuron, its protein molecule ion channels (Na^+ and K^+) being represented by conductances and its lipid bilayer by a capacitor [6]. Bursting activity in Hodgkin-Huxley models of neuronal activity is usually included through additional calcium currents [7]. Moreover, bursting behavior can be also related to persistent Na^+ currents in the pre-Botzinger complex [8–10], in the mesencephalic trigeminal sensory neuron [11], and M-currents in the hippocampus [12]. Other Hodgkin-Huxley-type models in which bursting activity appears can be found in Refs. [13,14].

Bursting activity can be also observed in thermally sensitive neurons: A Hodgkin-Huxley-type model of thermally sensitive neurons has been proposed by Huber and Braun [15–17], which describes spike train patterns experimentally observed in facial cold receptors and hypothalamic neurons of the rat [18], electroreceptor organs of freshwater catfish [19], and caudal photoreceptors of the crayfish [20]. There have been studied time delay- and coupling strength-induced synchronization transitions in scale-free networks of thermally sensitive neurons [21]. The synchronous behavior of two coupled thermally sensitive neurons has been numerically investigated as a function of the coupling strength, exhibiting a transition between a tonic firing and a bursting behavior [22].

The existence of a slow time scale in coupled bursting neurons enables us to define a bursting phase and frequency (its time rate) for each of them, even though on the spiking time scale they behave asynchronously [23]. The adjustment of the bursting phases and frequencies of two or more neurons can be treated as an example of chaotic phase synchronization, or the occurrence of a certain relation between phases of interacting systems, bursting neurons in our case, while the amplitudes (related to the spiking time scales) can remain chaotic and uncorrelated [24]. The presence of synchronized rhythms has been experimentally observed in electroencephalograph recordings of electrical activity in the brain, in the form of an oscillatory behavior generated by the correlated discharge of populations of neurons across the cerebral cortex [25].

Some types of synchronization of bursting neurons are thought to play a key role in Parkinson's disease [26,27], essential tremor [28], and epilepsy [29]. Hence, a possible way to control pathological rhythms would be to suppress the synchronized behavior. This can be obtained through application of an external high-frequency signal, and it constitutes the main goal of the deep-brain stimulation technique [30,31]. Deep-brain stimulation consists of the application of depth electrodes implanted in target areas of the brain like the thalamic *ventralis intermedius* nucleus or the subthalamic nucleus [32]. The overall effects of deep-brain stimulations are similar to those produced by tissue lesioning and have proved to be effective in suppression of the activity of the

---

*Corresponding author: viana@fisica.ufpr.br

pacemakerlike cluster of synchronously firing neurons, so achieving a suppression of the peripheral tremor [26].

While most progress in this field has come from empirical observations made during stereotactic neurosurgery, methods of nonlinear dynamics are beginning to be applied to understand this suppression behavior. In this work we consider a neuronal network model of thermally sensitive neurons (which display bursting activity) described by the Huber-Braun model [15–17]. We consider the existence of chemical synapses among neurons, for which the transmission times are important factors to be taken into account, when compared with gap-junction (electrical) coupling [33]. Chemical synapses can describe the connections of physically distant neurons, so we describe a connection architecture which enables such long-range couplings. The synaptic dynamics simulates the impulsive effect of a presynaptic neuron on a postsynaptic one when the former fires a spike.

A computational model of a neural network consists of a network architecture, which specifies how neurons are connected, and a neuronal dynamics attached to each unit, or node. The connections among neurons (of electrical or chemical nature) are the links of this network. The network connection architecture we use in a given model depends critically on the level of description we aim to develop for the neural network. The most fundamental level of description is the network of individual neurons. The human brain consists of approximately 10^{11} neurons, linked together by 10^{14} to 10^{15} connections, amounting to nearly 10^4 synapses per neuron [3]. This makes a detailed description of the brain a task yet beyond our ability. It is only in simpler species, like the worm *C. elegans*, that this description is feasible for studies of computational neuroscience [34].

However, neuroanatomic studies reveal that neurons with similar connectional and functional features are grouped into clusters with 10^5 to 10^6 cells with spatial localization. Such clusters form structures called cortical areas or subcortical nuclei [35,36]. A second level of description is, thus, a network whose nodes are the cortical areas, linked by axon fibers. For a few species anatomical data are available, e.g., the cat and the macaque monkey [37–40]. These descriptions have encouraged the use of clustered networks, or networks of networks, each cluster describing a cortical area with a given number of neurons [41].

In any level of description, we expect that the connection architecture of a neural network displays some distinctive statistical properties, related to graph-theoretical concepts. It is known that, in real neural networks, neurons are neither completely nor randomly connected. Studies of connectivity of some neural networks in both the microscopic (*C. elegans*) and the mesoscopic (cat corticocortical matrix) suggest that the networks exhibit the so-called small-world (SW) property, since they display features of both regular and random lattices [42].

Here we consider a SW network, consisting of a lattice in which each neuron has both local and nonlocal connections [43]. A neuron is connected to its nearest and next-to-nearest neighbors, as well as to a small number of randomly chosen nonlocal neurons [42]. It can be shown that the resulting network has a small average path length, in the same way that random networks do, but still retaining an appreciable degree of clustering, as in regular lattices [44].

In this work we consider the control (or suppression) of bursting synchronization using two types of control strategies. The first technique is to apply a time-periodic harmonic signal of fixed frequency and amplitude to one or more selected neurons [45]. Another strategy, proposed by Rosenblum and Pikovsky [46–48], makes this external signal depend on a mean-field behavior of the lattice at nearby times: a time-delayed feedback control procedure. We compare the application of this time-delayed feedback through different protocols. Both types of control procedures have been applied to networks of bursting neurons using Hodgkin-Huxley-type models of thermally sensitive neurons, where the synapses were supposed to be of a chemical nature.

The structure of this paper is as follows. In Sec. II we present the model of thermally sensitive neurons to be used in numerical simulations. Section III deals with the coupled neural network and the existence of bursting synchronization, studied by means of a conveniently defined geometrical phase. Section IV considers the control of bursting synchronization through an external time-periodic signal, and Sec. V studies the control performed by a time-delayed feedback signal. Our conclusions are left to the last section.

II. NEURONAL DYNAMICS

In the following we describe briefly the equations and parameters of the Huber-Braun model for thermally sensitive neurons. More details on the model can be found in Refs. [15,16,20]. The main dynamical variable for the ith neuron, belonging to a given network with $i = 1, 2, \ldots, N$, is the membrane potential V_i, whose time evolution is influenced by a number of currents from different sources, in the form (the membrane potential is measured in mV and time in ms)

$$C_M \frac{dV_i}{dt} = -I_{i\mathrm{Na}} - I_{i\mathrm{K}} - I_{isd} - I_{isa} - I_{i\ell}, \qquad (1)$$

where C_M is the membrane capacitance. $I_{i\mathrm{Na}}$, $I_{i\mathrm{K}}$, and $I_{i\ell}$ are, respectively, the Na$^+$ and K$^+$ ionic currents and the leak current, like in the Hodgkin-Huxley model (currents, or rather, current densities, are measured in $\mu\mathrm{A/cm}^2$). The currents I_{isd} and I_{isa} refer to intrinsic subthreshold oscillations: I_{isd} to the intrinsic membrane depolarization current and I_{isa} to the repolarization oscillations.

We associate a given conductance (measured in mS/cm^2) to each current in the following form:

$$I_{i\mathrm{Na}} = \rho g_{\mathrm{Na}} a_{\mathrm{Na}} (V_i - V_{\mathrm{Na}}), \qquad (2)$$

$$I_{i\mathrm{K}} = \rho g_{\mathrm{K}} a_{\mathrm{K}} (V_i - V_{\mathrm{K}}), \qquad (3)$$

$$I_{isd} = \rho g_{sd} a_{sd} (V_i - V_{sd}), \qquad (4)$$

$$I_{isa} = \rho g_{sa} a_{sa} (V_i - V_{sa}), \qquad (5)$$

$$I_{i\ell} = \rho g_\ell (V_i - V_\ell), \qquad (6)$$

where g_{Na}, g_{K}, g_{sd}, g_{sa}, and g_ℓ are the maximal conductances, and the reversal (Nernst) potentials for each ionic current are denoted by V_{Na}, V_{K}, V_{sd}, V_{sa} and V_ℓ.

It turns out that I_{Na} and I_{K} are simplified fast Hodgkin-Huxley currents representing Na$^+$ and K$^+$ channels, respectively. These fast currents are responsible for spike generation [20]. I_{sd} and I_{sa} are slow currents which are responsible for

TABLE I. Parameter values of the neuronal dynamics model according to Ref. [20].

Membrane capacitance	$C_M = 1.0 \ \mu\text{F/cm}^2$			
Conductances (mS/cm^2)				
$g_{\text{Na}} = 1.5$	$g_{\text{K}} = 2.0$	$g_{sd} = 0.25$	$g_{sa} = 0.4$	$g_\ell = 0.1$
Characteristic times (ms)				
$\tau_{\text{Na}} = 0.05$	$\tau_{\text{K}} = 2.0$	$\tau_{sd} = 10$	$\tau_{sa} = 20$	
Reversal potentials (mV)				
$V_{\text{Na}} = 50$	$V_{sd} = 50$	$V_{\text{K}} = -90$	$V_{sa} = -90$	$V_\ell = -60$
$V_{0\text{Na}} = -25$	$V_{0\text{K}} = -25$	$V_{0sd} = -40$		
Other parameters				
$\rho_0 = 1.3$	$\phi_0 = 3.0$	$T_0 = 20\,^\circ\text{C}$	$\tau_0 = 10$	$\eta = 0.012 \ \mu\text{A}$
$\gamma = 0.17$	$s_{\text{Na}} = 0.25$	$s_{\text{K}} = 0.25$	$s_{sd} = 0.09$	

subthreshold activation; i.e., they activate more slowly at lower membrane potentials [15]. These slow currents are necessary to generate bursting behavior.

We would like to remark that I_{sd} represents a generic voltage-gated Ca^{2+} channel and I_{sa} a current with behavior reminiscent of SK channels. However, while real SK channels are Ca^{2+}-sensitive rather than voltage-sensitive, the combination of I_{sa} and I_{sd} present in this model yields a behavior similar to voltage-gated Ca^{2+} channels coupled with SK channels. This procedure of replacing an ion-sensitive with a voltage-gated channel is common in biophysical models of neurons: For example, the inactivation of fast Na$^+$ channels is not really voltage-gated, but it is modeled this way in many models of neuronal dynamics. Hence, this model represents SK channels as voltage-sensitive because I_{sa} reasonably behaves like SK without the need for keeping track of intracellular Ca^{2+}.

For thermally sensitive neurons ρ is a scale factor depending on the temperature T which, for the kinetic ion model, is

$$\rho = \rho_0^{\frac{(T-T_0)}{\tau_0}}, \tag{7}$$

where ρ_0, T_0, and τ_0 are parameters.

The activation currents a_{Na}, a_{K}, a_{sd}, and a_{sa} have their evolution described by the differential equations

$$\frac{da_{\text{Na}}}{dt} = \frac{\phi}{\tau_{\text{Na}}}(a_{\text{Na},\infty} - a_{\text{Na}}), \tag{8}$$

$$\frac{da_{\text{K}}}{dt} = \frac{\phi}{\tau_{\text{K}}}(a_{\text{K},\infty} - a_{\text{K}}), \tag{9}$$

$$\frac{da_{sd}}{dt} = \frac{\phi}{\tau_{sd}}(a_{sd,\infty} - a_{sd}), \tag{10}$$

$$\frac{da_{sa}}{dt} = \frac{\phi}{\tau_{sa}}(-\eta I_{sd} - \gamma a_{sa}), \tag{11}$$

where τ_{Na}, τ_{K}, τ_{sd}, and τ_{sa} are characteristic times, and η, γ are other parameters, and we define a second temperature-dependent scale factor,

$$\phi = \phi_0^{\frac{(T-T_0)}{\tau_0}}. \tag{12}$$

Any inactivation of the ionic channels are neglected [15]. The factor η serves for increasing Ca^{2+} concentration following I_{sa}, and γ accounts for active elimination of intracellular Ca^{2+}.

The activation functions in the stable state, namely $a_{\text{Na},\infty}$, $a_{\text{K},\infty}$, $a_{sd,\infty}$, are related to the membrane potential by sigmoid functions:

$$a_{\text{Na},\infty} = \frac{1}{1 + \exp[-s_{\text{Na}}(V_i - V_{0\text{Na}})]}, \tag{13}$$

$$a_{\text{K},\infty} = \frac{1}{1 + \exp[-s_{\text{K}}(V_i - V_{0\text{K}})]}, \tag{14}$$

$$a_{sd,\infty} = \frac{1}{1 + \exp[-s_{sd}(V_i - V_{0sd})]}, \tag{15}$$

where s_{Na}, s_{K}, and s_{sd} are constants and $V_{0\text{Na}}$, $V_{0\text{K}}$, and V_{0sd} are activation voltages. The parameter values to be used in this paper are listed in Table I. The temperature we use in numerical simulations is $T = 8.0\,^\circ\text{C}$, for which we find bursting behavior characterized by repetitive spiking and the interspike interval (ISI) exhibits a chaotic evolution, followed by a quiescent regime [49–54]. A detailed analysis of the dependence of the neuron behavior with the temperature can be found in Ref. [20].

A representative example of bursting is shown in Fig. 1(a): The membrane potential of a single neuron described by the
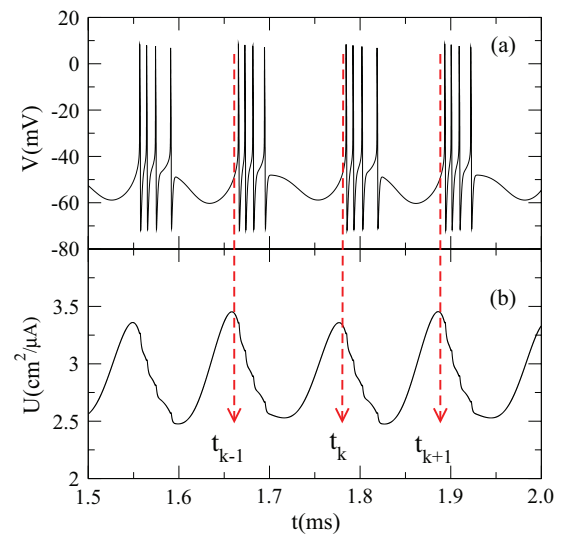
FIG. 1. (Color online) Time evolution of the (a) membrane potential (b) recovery variable (inverse of the subthreshold repolarization current) for an isolated neuron at temperature $T = 8.0\,^\circ\text{C}$. Other numerical parameters are listed in Table I. The red arrows indicate the times at which bursting cycles begin.
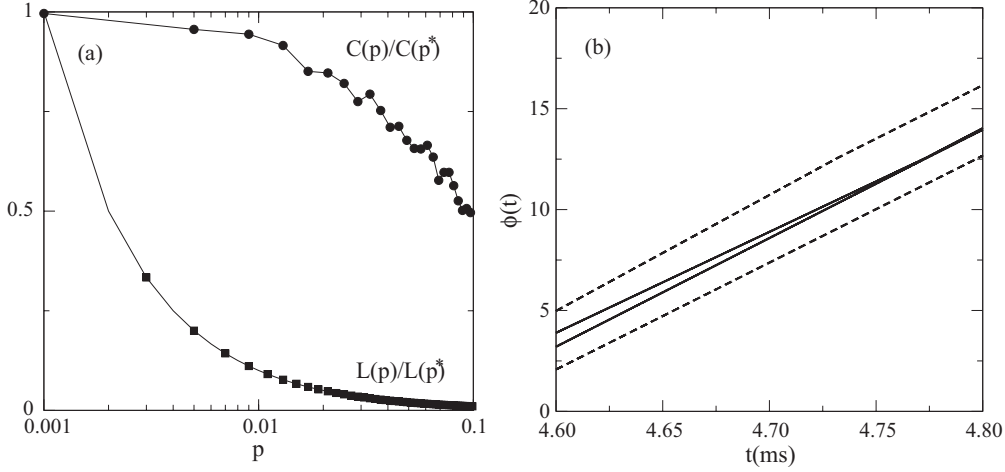
FIG. 2. (a) Normalized clustering coefficient (circles) and normalized average path length (squares) as a function of the probability of nonlocal shortcuts for a network with $N = 2000$ nodes. The reference probability is $p^* = 0.001$, with $L(p^*) = 1.0 \times 10^{-6}$ and $C(p^*) = 2.0 \times 10^{-6}$. (b) Time evolution of the bursting phase of two selected neurons in a SW network with $p = 0.01$. Dashed lines stand for uncoupled neurons; solid lines are for coupled neurons with $g_c = 0.01$ mS/cm^2.

Huber-Braun model undergoes repetitive spiking after periods of quiescent behavior. The beginning of each outburst of repetitive spiking is also a local maximum of the recovery variable $U = 1/I_{isa}$ and may be considered as the beginning of a bursting cycle [Fig. 1(b)]. This makes it possible to define a geometric phase. Let t_k be the time at which a kth bursting cycle begins. The phase is obtained by simple interpolation as [23]

$$\varphi(t) = 2\pi k + 2\pi \frac{t - t_k}{t_{k+1} - t_k}, \quad (t_k < t < t_{k+1}), \qquad (16)$$

and increases monotonically with time. However, due to the chaotic evolution of the membrane potential related to repetitive spiking, it turns out that the interval $t_{k+1} - t_k$ is different for each burst. Hence, a bursting frequency,

$$\Omega = \frac{d\varphi}{dt} \doteq \frac{\varphi(t) - \varphi(0)}{t}, \qquad (17)$$

gives the time rate of the phase evolution (in kHz).

III. NETWORK CONNECTIVITY

Two key quantificators for complex networks are their average distance between nodes L and the clustering coefficient C. The latter, roughly speaking, is the degree of overlap between neighborhoods of different sites. In other words, if we have a given node i connected to two other nodes j and k, C gives a probability that the nodes j and k are themselves connected. Small-world networks are characterized by small L values and a relatively large C value. Regular lattices have large values for C, but they have local connections only, which accounts for a large value of L. In contrast, random networks have small values for both L and C [43]. This suggests that SW networks are between these two limiting situations. We obtained SW networks following a procedure from Newman and Watts [55]: We start from a regular lattice with nearest neighbors and next-nearest neighbors; then we add nonlocal shortcuts in this lattice with a probability p. These shortcuts are ultimately responsible for diminishing the average

path length in the network, whereas the nearest neighbors account for the large clustering coefficient displayed by SW networks.

Hence, the two parameters characterizing the network architecture to be used are the number of neurons N and the probability of nonlocal shortcuts p. The network connectivity can be described by the adjacency matrix a_{ij} whose elements are equal to 1 (0), if the neurons i and j are (are not) connected. If the probability p is small, this matrix is band-diagonal and presents sparse nonzero elements at both sides. In Fig. 2(a) we plot the normalized clustering coefficient $C(p)/C(p^*)$ (where $p^* = 0.001$) and the normalized average path length $L(p)/L(p^*)$ as a function of the probability of nonlocal shortcuts for a network with $N = 2000$ nodes. We have chosen to work with $p = 0.01$, for which $C \sim 0.9$ is relatively large, whereas $L \sim 0.2$ is comparatively small, such that the conditions for a SW network are fairly fulfilled.

The coupling among neurons enters in the model through a synaptic current I_{syn} which is added in the differential equation (1) governing the behavior of the membrane potential for the ith neuron,

$$C_M \frac{dV_i}{dt} = -I_{i\text{Na}} - I_{i\text{K}} - I_{isd} - I_{isa} - I_{i\ell} - I_{\text{syn}}, \qquad (18)$$

where

$$I_{\text{syn}} = g_c \sum_{j=1}^{N} a_{ij} r_j(t)(V_{\text{syn}} - V_j), \qquad (19)$$

where g_c is a coupling strength with conductance dimensions, a_{ij} are the elements of the adjacency matrix, V_{syn} is the synaptic reverse potential, and $r_j(t)$ is the fraction of bond receptors of the jth neuron, whose time evolution is described by the differential equation ("synaptic dynamics") [56]

$$\frac{dr_j}{dt} = \left(\frac{1}{\tau_r} - \frac{1}{\tau_d} \right) \frac{1 - r_j}{1 + \exp(-V_j + V_0)} - \frac{r_j}{\tau_d}, \qquad (20)$$

where V_j is the membrane potential of the postsynaptic neuron and τ_r and τ_d are characteristic rise and decay times,

TABLE II. Parameter values for the synaptic dynamics according to Ref. [21].

Characteristic times (ms)	
$\tau_r = 0.5$	$\tau_d = 8$
Reversal potentials (mV)	
$V_{\text{syn}} = 20$	$V_0 = -20$

respectively, of the chemical synapse. The numerical values of the coupling parameters to be used in the simulations reported in this work can be found in Table II.

In the numerical simulations of SW networks of thermally sensitive neurons we use networks with $N = 2000$, with shortcut probability $p = 0.01$ and coupling strength $g_c = 0.01$ mS/cm^2, unless stated differently. Solving the coupled system of $5N$ equations (using a fourth-order Runge-Kutta method with fixed step size) yields $V_i(t)$ for each neuron, such that we can trace its time evolution and the times t_k at which the bursting cycles occur. After a sufficiently long integration we can retrace the time series and compute, using Eq. (16), the time evolution of the corresponding phase. The effect of coupling can be observed in Fig. 2(b), where we compare the phase evolution for two neurons when uncoupled (dashed lines) and after coupling (solid lines). It is clear that one of the effects of coupling is to induce phase synchronization of bursting, $\varphi_1(t) = \varphi_2(t) = \cdots \varphi_N(t)$, in such a way that the coupled neurons, even though not fully synchronized, are able to display a collective effect, bursting at the same time. The mean field of a network of synchronized bursters displays large-amplitude oscillations reflecting the coherent behavior of the assembly.

Two useful numerical diagnostics of bursting synchronization are the mean field of the network and Kuramoto's order parameter. The former is obtained by averaging the membrane voltages of all neurons belonging to the network at a given time: $V_m = (1/N)\sum_{i=1}^N V_i$. If the bursters are nonsynchronized, i.e., if they begin their bursting cycles at different times, the corresponding mean field exhibits small-amplitude noisy fluctuations with time. In a synchronized state, however, the mean field time evolution displays large-amplitude oscillations. The expected effect of the control is thus the reduction to minimal levels of the network mean field.

The complex phase order parameter is defined as [57]

$$z(t) = R(t)\exp(i\,\Phi(t)) \equiv \frac{1}{N}\sum_{j=1}^N \exp(i\varphi_j(t)), \qquad (21)$$

where R and Φ are the amplitude and angle, respectively, of a centroid phase vector for a one-dimensional lattice with periodic boundary conditions. If the neurons are uncoupled, for example, their bursting phases $\varphi_i(t)$ are expected to be uncorrelated such that their contribution to the result of the summation in Eq. (21) is typically small (due to statistical coincidences). In the limit of an infinite site ($N \to \infty$) we expect $R(t)$ to vanish. On the other hand, in a completely phase synchronized state the order parameter magnitude asymptotes the unity, indicating a coherent superposition of the phase vectors at each time. We usually compute the time-averaged order parameter magnitude $\overline{R} = \lim_{T\to\infty}(1/T)\int_0^T R(t)dt$.
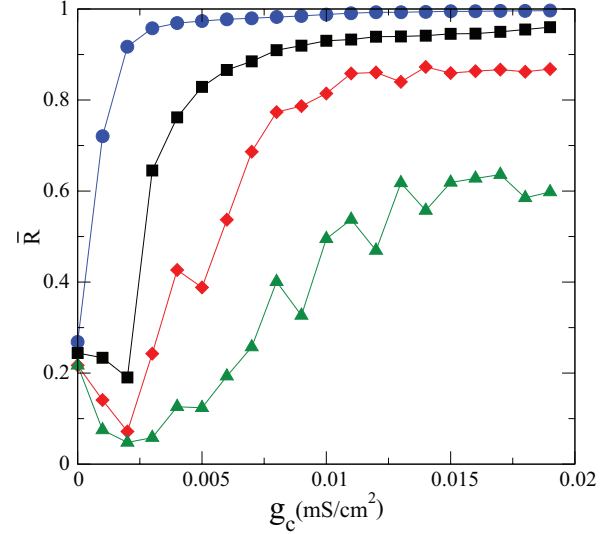
FIG. 3. (Color online) Time-averaged order parameter magnitude as a function of the coupling strength for SW networks with different values of the shortcut probability p: 0.0001 (green triangles), 0.001 (red diamonds), 0.004 (black squares), 0.020 (blue circles).

The time-averaged order parameter magnitude is plotted, in Fig. 3, against the coupling strength g_c, for SW networks with shortcut probabilities ranging from zero to 0.02. When the latter parameter is zero, the network has regular connections only, and thus it is unlikely to display synchronized behavior, if the coupling strength is small enough. In fact, $\overline{R}$ fluctuates between 0.05 and 0.60 in the coupling parameter range considered (green triangles in Fig. 3).

On the other hand, even a small probability is able to make at least part of the neurons to synchronize their bursting phases. For $p = 0.001$ (red diamonds in Fig. 3) and 0.004 (black squares in Fig. 3) a transition from a nonsynchronized to synchronized behavior is observed when g_c increases. The transition may occur for extremely small values of g_c, as when $p = 0.02$ (blue circles in Fig. 3).

From the above results, it is likely that the network (or at least parts of it) will synchronize if the coupling strength and the probability of nonlocal shortcuts is large enough. The synchronization of neuron activity has been related to some pathological rhythms like essential tremor and Parkinson's disease [26,32]. One strategy to diminish or suppress these oscillations is to apply some external intervention so as to take the network out of a synchronized state. This is the subject of the following sections.

IV. CONTROL THROUGH AN EXTERNAL TIME-PERIODIC SIGNAL

Inspired in techniques of deep-brain stimulation, in which an external time-periodic electric signal is applied to a cortical area to mitigate abnormal rhythms appearing in pathological conditions, we can investigate the control of bursting synchronization through a time-periodic signal with a given amplitude and frequency [29–31]. Such perturbation, when applied to an ensemble of Rulkov neurons [58,59] has been shown to produce global bursting frequency locking for scale-free

networks [60] and nonlocally coupled networks [61,62], as well as clusters of SW networks [45].

A time-periodic signal applied to a given neuron can be represented by an external injected current of amplitude I_0 (in $\mu A/cm^2$) and frequency ω (in kHz) of the form

$$I_{\text{ext}} = I_0 \sin(\omega t), \tag{22}$$

which is added to the right-hand side of Eq. (18). In strongly coupled networks (like globally or power-law coupled neurons) this intervention can be made on a single selected neuron. For scale-free networks, where there is a strongly connected hub, the latter can be the target of the intervention. In sparsely connected networks, like SW or random ones, it is unfeasible to randomly select a single neuron, since it is so poorly connected that a modification in its dynamics does not influence the network in a significant way. Hence, we choose to make the intervention in all neurons. This is biologically feasible since the electrodes injecting an ac current into a given region of the brain do modify the extracellular field potentials for a number of nearby neurons.

In order to investigate the effect of this external source we have used coupling strength values for which the unperturbed lattice ($I_0 = 0$) exhibits bursting synchronization. This synchronization between the bursting neurons and the external signal is possible due to the coupling effect on the triggering or termination of a burst in the individual neurons. A burst can be terminated (the neuron is driven to a quiescent state) if the external signal is positive. Conversely, a burst can be delayed if the signal is negative. The combination of these effects leads to the synchronization of the driven neuron with the signal. The effect of coupling, once it takes into account the mutual influences of all neurons in the network, is to change the mean field that each neuron feels.

When the bursting phases φ_i are equal, for a set of neurons, the corresponding frequencies $\Omega_i = \dot{\varphi}_i$ are likewise equal (the opposite is not necessarily true, though, for out-of-phase bursters can synchronize their frequencies, as is well known). The frequency mismatch $\Omega_i - \omega$ is plotted in Fig. 4 against the control frequency ω for different values of the control amplitude I_0. For each value of ω the bursting frequencies Ω_i are scattered over a relatively narrow interval, generating a fuzzy strip of points. The wider this strip, the less synchronized (in frequency) are the bursters. The difference $\Omega_i - \omega$ vanishes for a narrow interval of frequencies centered at $\omega = \omega_0 \approx 0.005$ kHz, indicating frequency locking with the external signal at frequencies around ~5 Hz [Fig. 4(a)].

Increasing the driving amplitude enlarges the frequency-locking interval [Figs. 4(a) and 4(b)]. For driving frequencies larger than those of this interval the strip of bursting frequencies is notably wide, indicating that the bursting neurons switch to frequencies different from those of the driving signal and of the other mutually synchronized bursters [23]. Figures 5(a) and 5(b) depict the time evolution of the external driving signal I_{ext} for $\omega = 8$ Hz, $I_0 = 0.10$ and 0.15 $\mu A/cm^2$, respectively. In the former case, the effect of the driving signal is weak, and we observe a small reduction in the mean field amplitude [Fig. 5(c)] and likewise a small decrease of the order parameter magnitude [Fig. 5(e)]. Actually the latter undergoes low-frequency oscillations, characterizing a kind of beat. For larger amplitude, however, the mean field
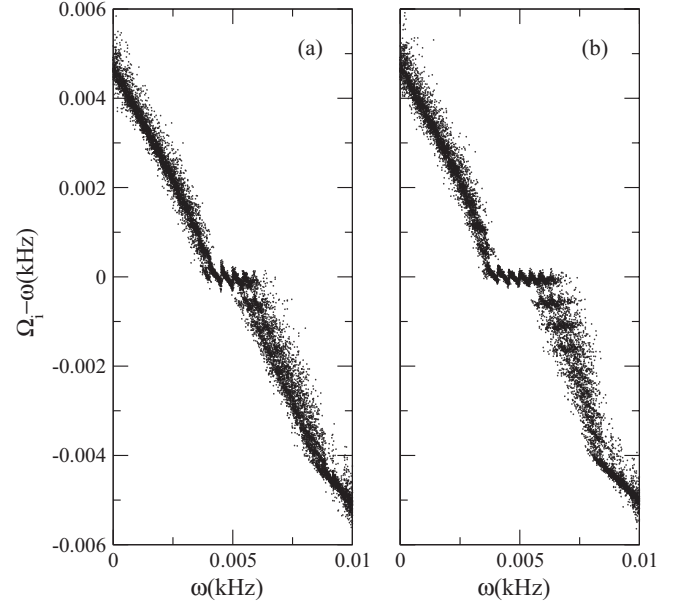
FIG. 4. Frequency mismatch of bursting neurons vs the external driving frequency for a SW network with $g_c = 0.01$ mS/cm^2, $p = 0.01$ and a driving signal with amplitude (a) $I_0 = 0.010$ $\mu A/cm^2$ and (b) $I_0 = 0.015$ $\mu A/cm^2$.

oscillation amplitudes decrease [Fig. 5(d)], indicating that the synchronized bursting is partially suppressed in this case. This observation is reinforced by the behavior of the order parameter [Fig. 5(f)], although with the same kind of beat.

Now we consider the effect of a driving signal with frequencies inside the locking interval ($\omega = 5$ Hz) and at the left-hand side of it ($\omega = 1$ Hz). These two cases, with the driving amplitude unchanged, are considered in Figs. 6(a) and 6(b),
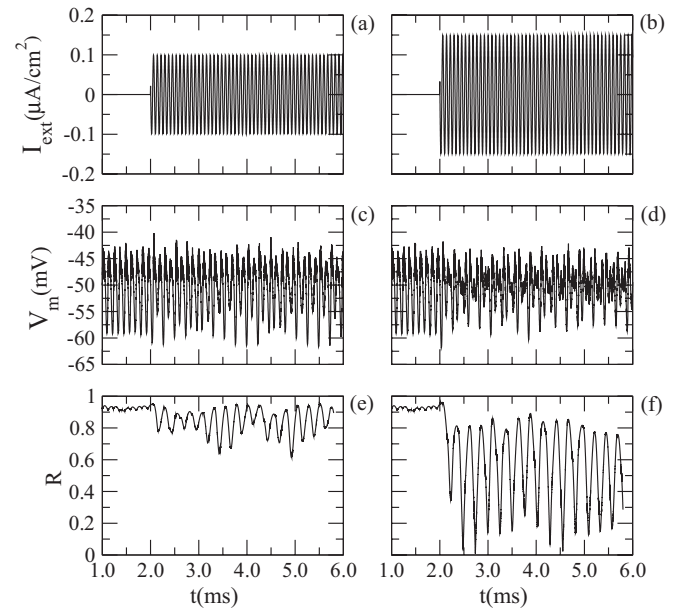
FIG. 5. Time evolution of the external driving signal I_{ext} [(a) and (b)], mean field [(c) and (d)], and order parameter magnitude [(e) and (f)] for $\omega = 8$ Hz, $I_0 = 0.10$ $\mu A/cm^2$ [(a), (c), and (e)], and $I_0 = 0.15$ $\mu A/cm^2$ [(b), (d), and (f)].
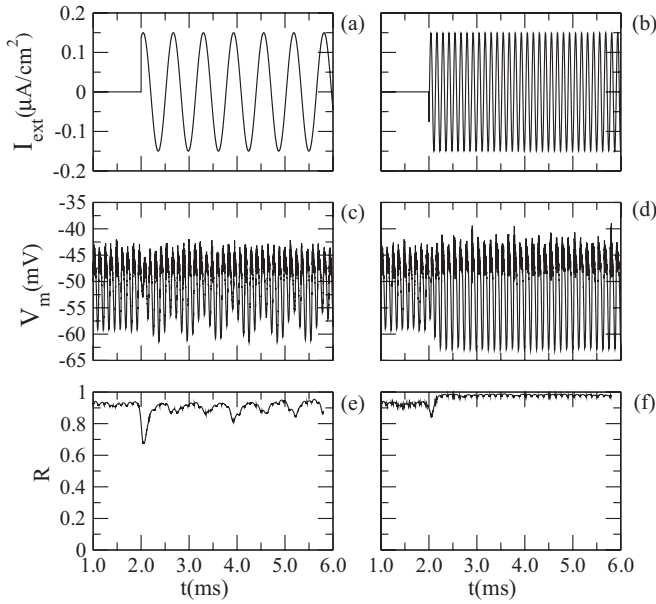
FIG. 6. Time evolution of the external driving signal I_{ext} [(a) and (b)], mean field [(c) and (d)], and order parameter magnitude [(e) and (f)] for $I_0 = 0.15\ \mu A/cm^2$ and $\omega = 1$ Hz [(a), (c), and (e)] and $\omega = 5$ Hz [(b), (d), and (f)].

respectively. In both cases there is no noticeable change in the oscillations of the network mean field [Figs. 6(c) and 6(d)], indicating that the synchronized state is not affected by the control signal for such frequencies, a conclusion supported by the order parameter magnitude [Figs. 6(e) and 6(f)].

It turns out that a detailed knowledge of the frequency-locking region, in the amplitude vs frequency diagram, is essential to design a proper application of the external control signal. In this diagram the frequency-locking regions are represented by an Arnold-like tongue similar to that obtained for periodically forced oscillators [Fig. 7(a)]. The width of this Arnold tongue $\Delta\omega$, increases with the signal amplitude [Fig. 7(b)]. The wider the frequency-locking interval is, the more robust is the external driving with respect to imperfect

parameter determination and noise, which is a question of considerable experimental importance.

The tongue is clearly asymmetric for small amplitudes, for its left boundary is steeper than the right one. In order to characterize quantitatively this asymmetry we also define a partial width $\delta\omega$ with respect to the center ω_0 of the locking frequency interval [Fig. 7(b)], which also increases with d, whereas its complement $\Delta\omega - \delta\omega$ practically does not increase with I_0, as can also be seen in the left boundary of the tongue depicted in Fig. 7(a).

V. CONTROL THROUGH A TIME-DELAYED FEEDBACK SIGNAL

The use of an external input as a control device for neuron bursting involves a number of problems related with the choice of parameters, especially the amplitude and frequency. If the amplitude of the external signal is too large, for example, we could have neuron damage, and if the frequency falls inside a given mode-locking tongue (or, as we have seen, at its left-hand side also) we would have practically no effect in terms of control. Another procedure to accomplish bursting control consists of using a time-delayed feedback signal. This has the advantage of always working with signals of appropriate intensity, and it has been shown to be capable to suppress chaotic bursting synchronization in neuronal networks with several types of coupling: global (all-to-all) [46,47], random [48], and scale-free [63].

According to the value that the mean field takes on for a given time t and its value at an earlier time τ (the control delay), we can design a feedback signal to be applied to the network so as to drive the system out of a synchronized state. This is feasible if a probe is inserted in the network measuring the mean field at different times, and integrating the effect of time-delayed values into a feedback scheme which applies to the network a control signal. The latter is similar in essence to the one studied in the previous section, but its amplitude and frequency are no longer constants but instead determined by the network dynamics itself.
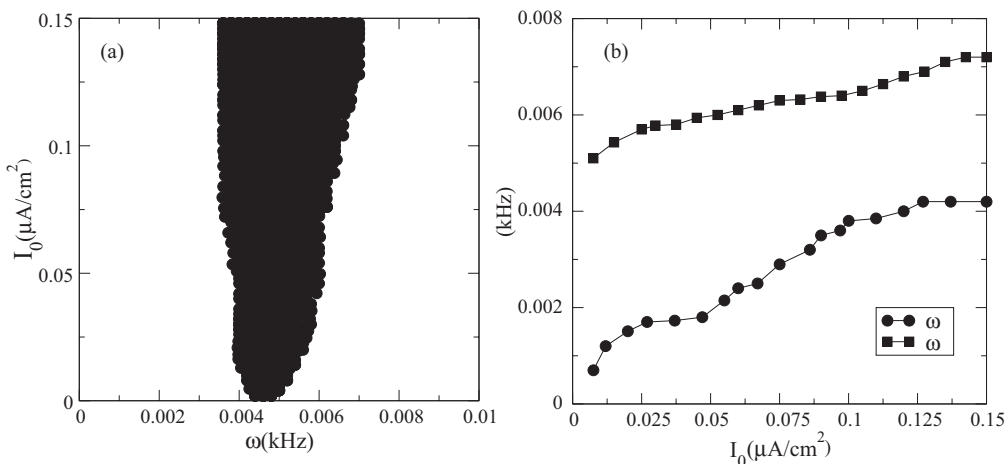
FIG. 7. (a) Arnold-like tongue of frequency locking for coupled bursting neurons in a SW network. (b) Full width (squares) and partial width (circles) of the mode-locking tongue as a function of the driving amplitude.

Let $V_m(t)$ and $V_m(t - \tau)$ be the neuronal mean field measured at two times with a delay τ (measured in ms). The feedback electric signal is

$$I_{\text{feed}} = g_f[V_m(t - \tau) - V_m(t)], \qquad (23)$$

where g_f is a control amplitude (also with conductance dimensions), which may or may not vary during the application, according to the protocol used. The intensity of the control signal is thus proportional to the difference between the actual mean field and the time-delayed one. Let us consider first the case in which the network is nonsynchronized: the mean field presents small-amplitude fluctuations during an arbitrarily large time. Hence, the difference $V_m(t - \tau) - V_m(t)$ is likely to be small, and practically no feedback is needed. On the other hand, if the network is synchronized the oscillations in the mean field makes the difference large in general, and the intensity of the control signal is proportional to this difference. As the control drives the network out of a synchronized state, the mean field oscillations become smaller and thus the control signal itself does not need to be as strong as before.

A. Free-running feedback signal

The effect of a free-running time-delayed feedback signal is illustrated by Fig. 8, obtained for two different values of g_f and the same values of the time delay $\tau = 2$ ms. In Figs. 8(a) and 8(b) we plot the time evolution of the feedback signals I_{feed} for $g_f = 0.010$ mS/cm^2 and 0.015 mS/cm^2, respectively. We observe that, after the feedback signal is switched on, the oscillations of the mean field V_m are just slightly decreased for $g_f = 0.010$ mS/cm^2 [Fig. 8(c)] and much more diminished for 0.015 mS/cm^2 [Fig. 8(d)]. Indeed, after the beginning of the control the order parameter magnitude decreases to 0.8 in
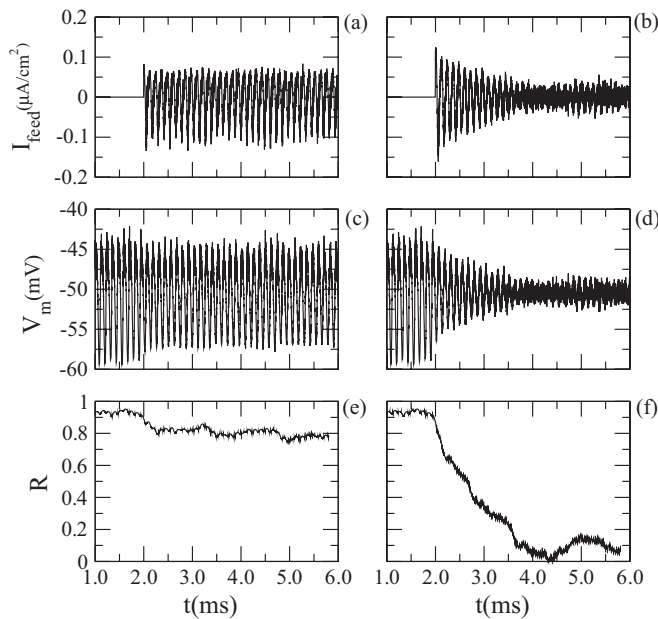
the former case [Fig. 8(e)] and to almost zero in the latter one [Fig. 8(f)].

B. Protocols for a smart feedback signal

Let us assume that the feedback circuitry necessary to the control procedure is designed to work as a kind of "smart" pacemaker. We can, in principle, program this pacemaker to obey a given control protocol, where we wish to comply with two basic characteristics: (i) The external signal must be as low as possible so as not to perturb too much the same neurons we want to control; (ii) the external signal must be kept small so as to conserve energy and prolong the battery life of the pacemaker. The criterion (i) is almost automatically satisfied for a time-delayed feedback signal, since the control signal (being proportional to the mean field) is never larger than the mean field for the values of g_f we used in our simulations. The criterion (ii) is somewhat more difficult to fulfill, so we need to compare different control protocols in order to measure how much energy they need to achieve a determined goal (in our case, an efficient suppression of synchronization).

1. Protocol 1

In the free-running operation, the control is always "on." An alternative procedure would be a pulsed operation, which we now consider. The first protocol (P1) consists on applying the feedback signal at a given time $t = t_i$ and switching it off, a short interval after, at $t = t_f$. As a representative example of the usefulness of this protocol to control bursting synchronization, we depict in Figs. 9(a) and 9(b) the time evolution of the time-delayed feedback signal I_{feed} for $g_f = 0.010$ mS/cm^2 and 0.015 mS/cm^2, respectively. In both cases the signal is switched on at $t_i = 2.0$ ms and switched off

FIG. 8. Time evolution of the free-running time-delayed feedback signal I_{feed} [(a) and (b)], mean field [(c) and (d)], and order parameter magnitude [(e) and (f)] for $g_c = 0.01$ mS/cm^2 [(a), (c), and (e)] and $g_c = 0.015$ mS/cm^2 [(b), (d), and (f)]. In both cases $\tau = 2$ ms.
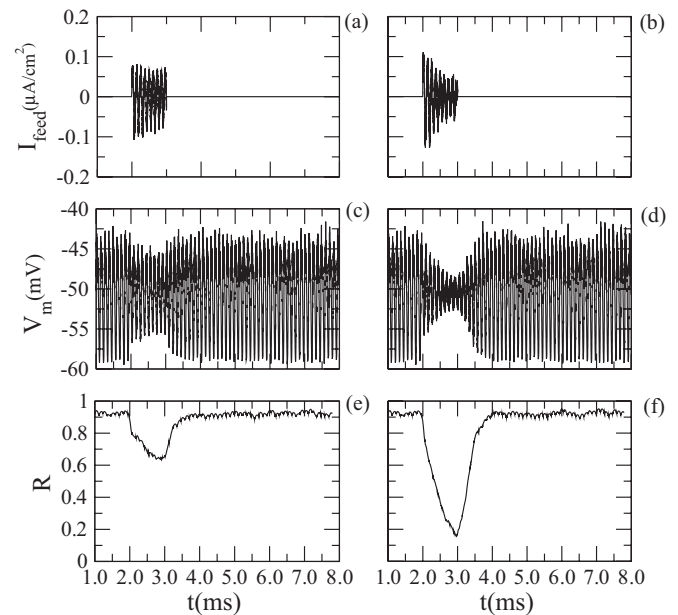
FIG. 9. Time evolution of the time-delayed feedback signal (protocol P1) I_{feed} [(a) and (b)], mean field [(c) and (d)], and the order parameter magnitude [(e) and (f)] for $g_c = 0.010$ mS/cm^2 [(a), (c), and (e)] and $g_c = 0.015$ mS/cm^2 [(b), (d), and (f)]. In both cases $\tau = 2$ ms.
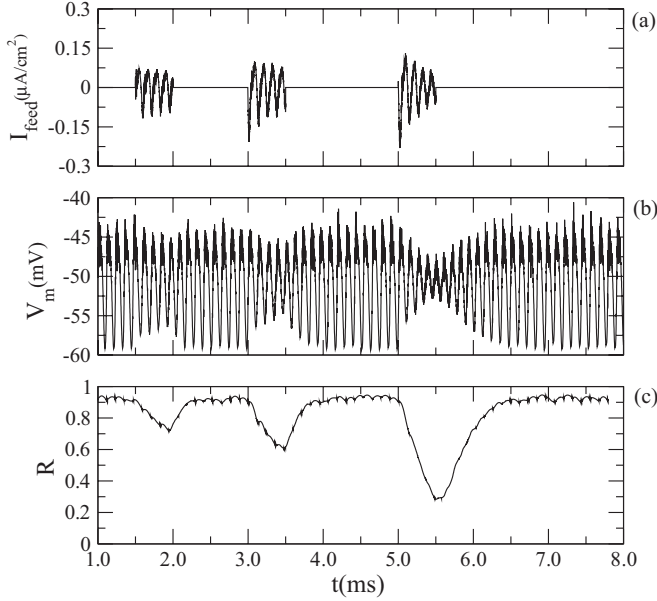
FIG. 10. Time evolution of the (a) time-delayed feedback signal (protocol P1) I_{feed}, (b) mean field, and (c) order parameter magnitude for three different values of the time delay: τ, 2τ, and 3τ, with $\tau = 10$ ms and $g_c = 0.010$ mS/cm^2.

FIG. 11. (Color online) Order parameter magnitude as a function of the time delay for different values of the control amplitude: $g_f = 0.005$ mS/cm^2 (black circles), $g_f = 0.010$ mS/cm^2 (green circles), $g_f = 0.015$ mS/cm^2 (red squares), and $g_f = 0.020$ mS/cm^2 (blue diamonds).

at $t_f = 3.0$ ms. The corresponding mean field, which has large-amplitude oscillations of ca. 15 mV amplitude (for the uncontrolled network), diminishes its amplitude to $\sim$10 mV [Fig. 9(c)] and $\sim$ 5 mV [Fig. 9(d)] as long as the control signal is applied. The order parameter decreases to 0.6 [Fig. 9(e)] and 0.2 [Fig. 9(f)] for these cases.

The control signal is oscillatory but its amplitude decreases during application since the network becomes more synchronized due to the control. Moreover, the network has a certain "inertia": After the control is switched on it takes a certain time to achieve a significant reduction in the mean field; after the control is switched off it takes a certain time for the network to resume its previous (synchronized) behavior. These effects are enhanced for increasing coupling strength [compare Figs. 9(c) and 9(d)].

In order to examine the influence of the time delay on the effectiveness of the feedback control through protocol P1, we switch on the control at $t_i = 1.5$ ms and switch it off at $t_f = 2.0$ ms, using a time delay $\tau = 1.0$ ms [Fig. 10(a)]. Then we repeat the application of control at times $t_i = 3.0$ and 5.0 ms with the same duration and with time delays 2τ and 3τ, respectively. In Fig. 10(b) we observe that the oscillations of the mean field decrease their amplitudes as τ is increased. Moreover, the order parameter plunges into smaller values as τ increases [Fig. 10(c)].

The results of Fig. 10 suggest that increasing the time delay is an efficient and "nonexpensive" way to achieve desynchronization of the network (instead of increasing the strength parameter g_f). In fact, as shown in Fig. 11, the mean order parameter magnitude of a controlled network decreases, as a general trend, with the time delay τ, for different values of the control amplitude g_f (the mean is computed as long as the control is applied). It is worth noting that, if the latter is too small, there is practically no effect of the time delay,
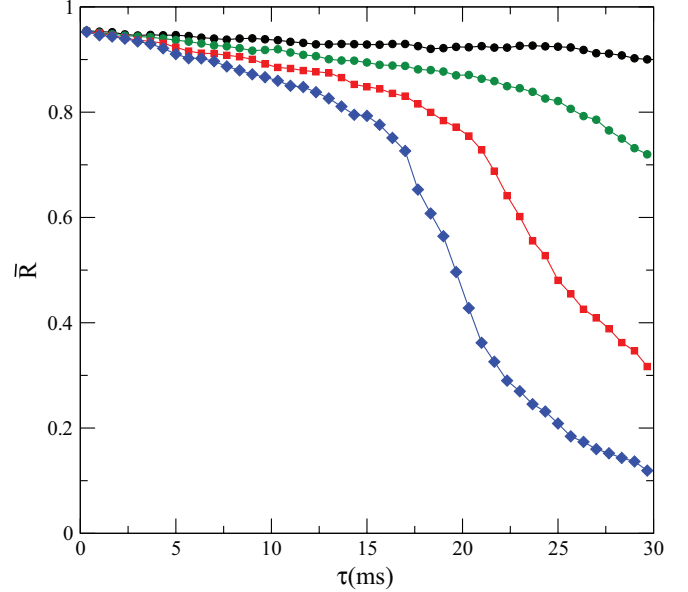
unless it is so large that it is unfeasible from the point of view of the simulation time (or the time of a hypothetic realistic application). We conclude that, for the time delay to play a significant role in the desynchronizing effect, the amplitude must be higher than $\sim$0.015 (indicated by red squares in Fig. 11).

The effectiveness of the control procedure on reducing or suppressing synchronization can be measured by the *suppression coefficient* [47],

$$S = \sqrt{\frac{\mathrm{Var}(V_{m0})}{\mathrm{Var}(V_{mf})}}, \qquad (24)$$

where V_{m0} and V_{mf} are the values of the mean field in the absence and presence of the control, respectively, and Var($\cdot$) stands for the variance of the mean field oscillations. The feedback scheme is ideally efficient when the variance of the controlled mean field vanishes, irrespective of its value without control, corresponding thus to an infinite value of S. As a general rule, the larger the value of S, the more efficient the feedback will be on suppressing synchronization. It is convenient to consider regions with large values of S, or domains of control, in the control parameter plane where the control strength g_f is plotted against the time delay τ.

Figure 12 displays the suppression coefficient for a time-delayed control signal as a function of g_f and τ, indicating that a good suppression of bursting synchronization is obtained for $g_f \gtrsim 0.012$ mS/cm^2 and $\tau \gtrsim 25$ ms. The protocol (P1) has the disadvantage of the control signal being applied irrespective of the value of the order parameter. This means that the control is continually applied even if the order parameter is small. We can devise other protocols to apply the control signal in a smart way from the point of view of energy saving, and
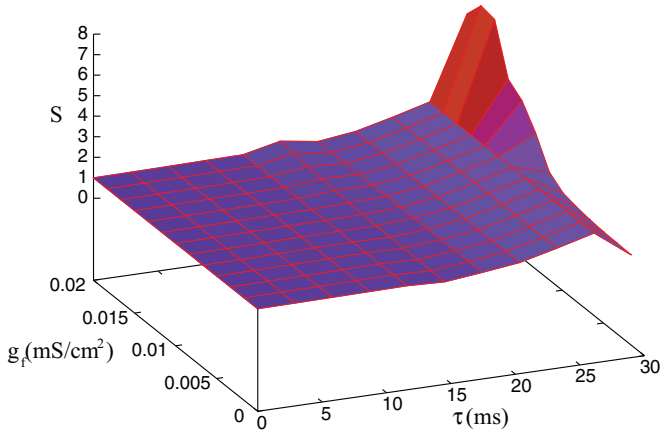
FIG. 12. (Color online) Suppression coefficient as a function of the control parameters (strength and time delay) for time-delayed feedback control (protocol P1).

based on monitoring the actual value of the order parameter. We propose the use of two such "smart" protocols.

2. Protocol 2

Here we establish the order parameter magnitude as a diagnostic tool of synchronization (it involves rather simple arithmetic operations which can be could be carried out by a microchip in the pacemaker circuitry, for example). We predefine, in a rather arbitrary way, values $\overline{R} > 0.95$ as characterizing a (global) synchronized state and values $\overline{R} < 0.4$ as characterizing a target nonsynchronized state, i.e., the goal which the control procedure is aimed to reach.

The second protocol (P2) is implemented as follows: The control is switched on, with a given strength g_f, only if the network order parameter magnitude becomes less or equal to $R_1 = 0.95$. This is a convenient value since, in practice, a synchronized network has $R \sim 0.95$ most of the time, with small fluctuations. As the neurons become nonsynchronized the order parameter begins to decrease and it is monitored until it reaches $R_2 = 0.40$; then it is switched off. Without control the network tends to resume, after some time, its previously synchronized state. Hence, when R increases past $R_3 = 0.50$ the control is switched on again with the same value of g_f as before.

While the uncontrolled mean field oscillation amplitudes lie in the $\sim$15-mV range, the controlled oscillations have roughly half this value [Fig. 13(a)], and the signal is applied in the form of short pulses of constant amplitude $g_f = g_c$ [Fig. 13(b)] according to the actual value of the order parameter magnitude [Fig. 13(c)], which oscillates between R_2 and R_3. These limits (but not necessarily their difference) can be lowered if we wish that the mean field oscillation amplitudes become even shorter.

3. Protocol 3

The third protocol (P3) is similar to P2: When $R \leqslant R_1$ the control is switched on until $R \leqslant R_2$, when it is switched off, and it is switched on again only if $R \geqslant R_3$ [Fig. 14(c)], with a similar decrease of the mean field oscillation amplitudes, when compared with P2 [Fig. 14(a)]. The difference with P2 lies in the intensity of the control signal. To further save energy, each
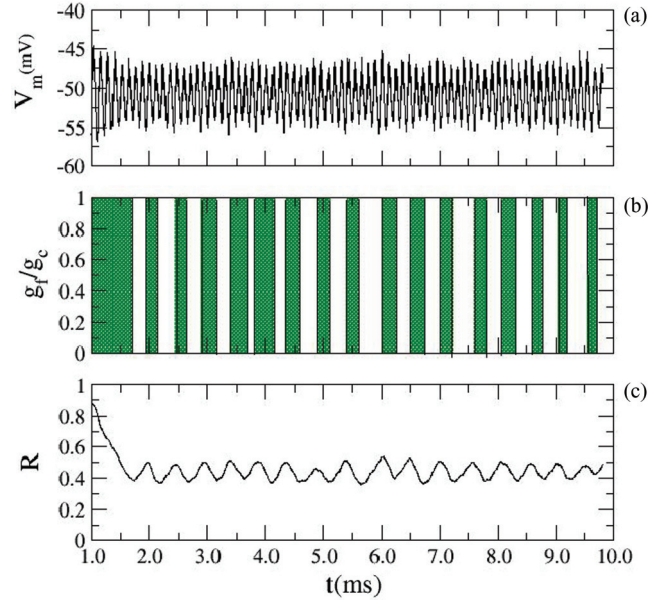
FIG. 13. (Color online) Time evolution of (a) mean field, (b) normalized control signal amplitude, and (c) order parameter magnitude for a time-delayed feedback signal applied according protocol P2, with $g_f = 0.012$ mS/cm^2 and $\tau = 1$ ms. The area under the control pulses is depicted in green.

time we switch on the control we use initially a very small value of g_f (say, 10% of g_c) and test whether or not R is kept smaller than R_3: If so, g_f is not altered; if not, we slightly increase g_f and test again, until we reach a satisfactory value, which is usually of the order of 50% of g_c [Fig. 14(b)].

However, since the control pulses in P3 are of lower amplitude than in P2, they have to be applied more often;
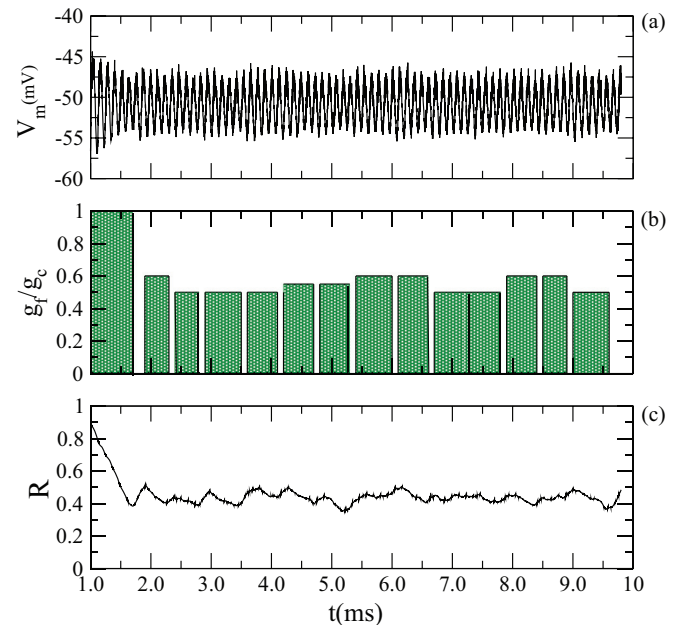
FIG. 14. (Color online) Time evolution of (a) mean field, (b) normalized control signal amplitude, (c) order parameter magnitude, for a time-delayed feedback signal applied according protocol P3, with $\tau = 1$ ms. The area under the control pulses is depicted in green.
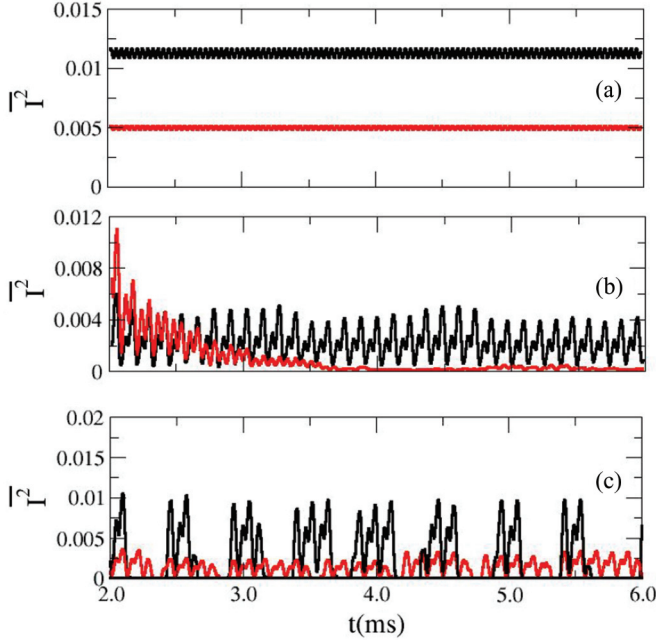
FIG. 15. (Color online) Running averages of the signal current squared $\overline{I^2}$ [measured in $(\mu A/cm^2)^2$] for (a) an external time-periodic signal, with $\omega = 8$ Hz, $I_0 = 0.010$ $\mu A/cm^2$ (red) and $I_0 = 0.015$ $\mu A/cm^2$ (black); (b) a free-running feedback signal, with $g_f = 0.015$ mS/cm^2, $\tau = 1$ ms (black) and 3 ms (red); (c) a feedback signal using the protocols P2 (black), and P3 (red).

i.e., the intervals between two pulses are shorter than for protocol P2. We integrated the area under the curve of the control pulses [depicted in green bars in Figs. 13(b) and 14(b)] in order to evaluate the "energy content" of the control signals according to the protocols P2 and P3, having the same interval $R_2 < R < R_3$ for the order parameter. This quantity has been found to be 36 400 for protocol P2 (Fig. 13) and 36 300 for P3 (Fig. 14), resulting in a slight advantage of P3 over P2.

4. Comparisons among different control procedures

A more direct way to compare the energy expenditure for the different control procedures we have introduced is to compute the power related to the injected currents, both the external time-periodic signal (22) and the time-delayed feedback signal (23). Assuming an effective conductance g_{eff}, the time-averaged power required for each signal is $P = \overline{I^2}/g_{\text{eff}}$. In Fig. 15 we plot the running average of the signal current squared $\overline{I^2}$ for a given time window. The actual energy consumed is proportional to the total area under the curves shown.

For the external signal (22) this quantity can be evaluated explicitly,

$$\overline{I^2} = \frac{I_0^2}{2}\left[1 - \frac{\sin(4\pi T/T_0)}{4\pi T/T_0}\right], \tag{25}$$

where T is the time window used for the running average and $T_0 = 2\pi/\omega$ is the natural period of the signal. When evaluating running averages it often turns out that $T \approx T_0$; hence, it results in a small amplitude oscillation around $I_0^2/4$. As a matter of fact, Fig. 15(a) shows the quantity $\overline{I^2}$ fluctuating around

0.005 $(\mu A/cm^2)^2$ for an amplitude $I_0 = 0.10$ $\mu A/cm^2$, and 0.012 $(\mu A/cm^2)^2$ for $I_0 = 0.15$ $\mu A/cm^2$. In Fig. 15(b) we have computed $\overline{I^2}$ for the free-running time-delayed feedback signal with $g_f = 0.015$ mS/cm^2, and $\tau = 1$ ms (red) and $\tau = 3$ ms (black). Since the value of $\overline{I^2}$ decreases exponentially with time for $\tau = 3$ ms it turns out that its effect, besides more efficient for suppressing synchronization, is also more energy saving than for $\tau = 1$ ms.

Finally, in Fig. 15(c) we compare the two protocols: P2 (black) with the $g_f = 0.015$ mS/cm^2 (as in Fig. 13); and P3 (red) (as in Fig. 14). For P2 we must keep in mind that g_f is not constant, whereas the time delay τ is the same for them. The area under the curve for P3 is shorter than for P2, which reinforces our earlier observation that P3 is slightly more energy saving than P2. As for the protocol P1, it cannot be directly compared with P2 and P3 because the times at which the control is switched on and switched off are rather arbitrary and do not follow the behavior of the order parameter magnitude, as P2 and P3 do.

VI. CONCLUSIONS

In this paper we studied the control of bursting synchronization of a neuronal network using a Hodgkin-Huxley-type model of coupled differential equations that mimics the dynamical behavior of signal transmission among thermally sensitive neurons with chemical coupling. We have considered networks of coupled thermally sensitive neurons, whereas most of the existing works on this model considered a small number of neurons. Moreover, up to now only the spiking regime has been investigated, and we found parameter values such that thermally sensitive neurons present a bursting regime with two time scales (a fast spiking scale and a slow bursting scale), in which a geometrical phase was identified, allowing studies of phase and frequency synchronization of the bursting activity.

We used a SW coupling architecture in which we have regular local connections among neighbor neurons as well as nonlocal shortcuts randomly chosen according to a given probability. This probability was chosen such that the average path length of the network is small, due to the nonlocal shortcuts, like in a random network, whereas the clustering coefficient is relatively large due to the local connections as in a regular network. We characterized bursting phase synchronization through: (i) the amplitude of the mean field oscillations of the network and (ii) the bursting phase and its corresponding order parameter magnitude.

We observed a transition between a nonsynchronized and a synchronized bursting as the coupling strength increases past a critical value. This value becomes smaller as the probability of nonlocal shortcuts is increased, and the network is so sensitive to them that, for as few as 3% of nonlocal shortcuts (in a network of $N = 2000$ neurons) the network already exhibits bursting synchronization for small coupling strengths. This suggests the strong influence of nonlocal coupling features in collective phenomena displayed by complex networks.

Synchronized bursting makes the network mean field exhibit large-amplitude oscillations that may be undesirable, as in the case of abnormal rhythms related to Parkinson's

disease and epileptic seizures. Hence, we studied procedures to control bursting synchronization so as to suppress or reduce it to tolerable levels. In this paper the numerical simulations were performed with a Hodgkin-Huxley-type model of thermally sensitive neurons. The temperature for which the bursting activity was found is lower than the physiological temperatures for Parkinsons disease and epileptic seizures. In spite of this, the model exhibits the same kind of behavior of other models for neuron dynamics where bursting synchronization has been described and studied, as the Hindmarch-Rose equations, the Bonhoeffer-Van der Pol model, and the Rulkov map [47].

One such procedure is to insert an external time-periodic control signal with constant amplitude and frequency. If the network is already synchronized we can view this external signal as a harmonic driving acting on a nonlinear oscillator, thus presenting the same kind of Arnold tongue behavior expected for such systems. In fact, we identified frequency-locking regions (tongues) in the control parameter plane and related their widths to the control amplitude. If we force the systems out of this frequency-locked state we can desynchronize a number of oscillators, in particular using frequencies higher than those belonging to the locking interval.

This external time-periodic signal has the disadvantage of having an amplitude which, if large enough, might damage the neurons on which the signal is being applied. An alternative procedure is to choose the signal amplitude according to the difference between the actual neuronal mean field and the mean field registered earlier (with a time delay τ), i.e., a time-delayed feedback signal which, by construction, has an amplitude typically smaller than the variable it intends to perturb. For example, if the action potential of the synchronized neurons vary between 0 (just before a spike) and -70 mV (in the refractory postspike state) a feedback control signal amounts to just $\sim$0.2 mV amplitude, which not only do not damage the neuron but also do not perturb it so to drive the neuron out of a bursting state.

In principle, the time-delayed feedback signal could be implemented through a pacemaker, and we proposed three different protocols for its use, besides the free-running application, taking into account the energy used to reduce bursting synchronization. In the first protocol we apply the control pulses at well-defined time intervals. We can control bursting synchronization by varying the time delay used in the feedback signal, and we showed that the order parameter can be made to vanish using a suitable value of τ. In particular, we identified the regions (in the control parameter plane) for which good suppression of synchronization is achieved.

Other protocols can be devised to save energy by applying the control signal only when the order parameter of the network is outside a specified range (of low values). In the second protocol we apply constant control pulses such that the order parameter is kept inside this range, and in a third protocol the minimum possible value of pulse amplitude is chosen for the same control goal. The latter protocol displays a slightly shorter energy consumption with respect to the former.

[1] R. F. Thompson, *The Brain: A Neuroscience Primer* (W. H. Freeman, New York, 2000).

[2] J. G. Nicholls, A. R. Martin, B. G. Wallace, and P. A. Fuchs, *From Neuron to Brain*, 4th ed. (Sinauer, Sunderland, MA, 2001).

[3] E. M. Izhikevich, *Dynamical Systems in Neuroscience: The Geometry of Excitability and Bursting* (The MIT Press, Cambridge, MA, 2007).

[4] M. F. Bear, B. W. Connors, and M. A. Paradisio, *Neuroscience: Exploring the Brain*, 3rd ed. (Lippincott, Williams & Wilkins, Philadelphia, 2007).

[5] S. Coombes and P. C. Bressloff (eds.), *Bursting: The Genesis of Rhythm in the Nervous System* (World Scientific, Singapore, 2005).

[6] A. L. Hodgkin and A. F. Huxley, J. Physiol. **117**, 500 (1952).

[7] P. R. Shorten and D. Wall, Bull. Math. Biol. **62**, 695 (2000).

[8] R. J. Butera, Jr., J. Rinzel, and J. C. Smith, J. Neurophysiol. **82**, 382 (1999).

[9] R. J. Butera, Jr., J. Rinzel, and J. C. Smith, J. Neurophysiol. **82**, 398 (1999).

[10] C. A. Del Negro, N. Koshiya, R. J. Butera, Jr., and J. C. Smith, J. Neurophysiol. **88**, 2242 (2002).

[11] N. Wu, A. Enomoto, S. Tanaka, C.-F. Hsiao, D. Q. Nykamp, E. Izhikevich, and S. H. Chandler, J. Neurophysiol. **93**, 2710 (2005).

[12] C. Yue and Y. Yaari, J. Neurosci. **24**, 4614 (2004).

[13] R. E. Plant and M. Kim, Biophys. J. **16**, 227 (1976).

[14] D. Roy and V. Jirsa, Frontiers in Computational Neuroscience **7**, 1 (2013).

[15] H. A. Braun, M. T. Huber, M. Dewald, K. Schäfer, and K. Voigt, Int. J. Bifurcat. Chaos **8**, 881 (1998).

[16] W. Braun, B. Eckhardt, H. A. Braun, and M. Huber, Phys. Rev. E **62**, 6352 (2000).

[17] H. A. Braun, M. T. Huber, N. Anthes, K. Voigt, A. Neiman, X. Pei, and F. Moss, BioSystems **62**, 99 (2001).

[18] H. A. Braun, M. Dewald, K. Schäfer, K. Voigt, X. Pei, K. Dolan, and F. Moss, J. Comput. Neurosci. **7**, 17 (1999).

[19] K. Schäfer, H. A. Braun, R. C. Peters, and F. Bretschneider, Pflgers Arch.- Eur. J. Physiol. **429**, 378 (1995).

[20] U. Feudel, A. Neiman, X. Pei, W. Wojtenek, H. Braun, M. Huber, and F. Moss, Chaos **10**, 231 (2000).

[21] Y. Hao, Y. Gong, L. Wang, X. Ma, and C. Yang, Chaos Solitons Fractals **44**, 260 (2011).

[22] S. Postnova, K. Voigt, and H. A. Braun, J. Biol. Phys. **33**, 129 (2007).

[23] M. V. Ivanchenko, G. V. Osipov, V. D. Shalfeev, and J. Kurths, Phys. Rev. Lett. **93**, 134101 (2004).

[24] A. Pikovsky, M. Rosenblum, and J. Kurths, *Synchronization: A Universal Concept in Nonlinear Sciences* (Cambridge University Press, Cambridge, UK, 2001).

[25] M. Steriade, F. Amzica, and D. Contreras, J. Neurosci. **16**, 392 (1996).

[26] M. S. Titcombe, L. Glass, D. Guehl, and A. Beuter, Chaos **11**, 766 (2001)

[27] C. Hammond, H. Bergman, and P. Brown, Trends Neurosci. **30**, 357 (2007).

[28] A. Schnitzler, C. Münks, M. Butz, L. Timmermann, and J. Gross, Movement Disorders **24**, 1629 (2009).

[29] L. B. Good, S. Sabesan, S. T. Marsh, K. Tsakalis, D. Treiman, and L. Iasemidis, Int. J. Neural Syst. **19**, 173 (2009).

[30] J. Y. K. Lee and D. Kondziolka, J. Neurosurg. **103**, 400 (2005).

[31] J. Modolo, J. Henry, and A. Beuter, J. Biol. Phys. **34**, 351 (2008).

[32] A. Beuter, M. S. Titcombe, F. Richer, C. Gross, and D. Guehl, Thalamus Relat. Syst. **1**, 203 (2001).

[33] E. R. Kandel, J. H. Schwartz, and T. M. Jessell, *Principles of Neural Science*, 4th ed. (McGraw-Hill, New York, 2000).

[34] L. R. Varshney, B. L. Chen, E. Paniagua, D. H. Hall, and D. B. Chklovskii, PLoS Comput. Biol. **7**, e1001066 (2011).

[35] C. C. Hilgetag and M. Kaiser, in *Lectures in Supercomputational Neuroscience (Dynamics in Complex Brain Networks)*, edited by P. B. Graben, C. Zhou, M. Thiel, and J. Kurths (Springer, Berlin-Heidelberg-New York, 2008).

[36] G. Zamora-López, C. Zhou, and J. Kurths, Chaos **19**, 015117 (2009).

[37] J. W. Scannell and M. P. Young, Curr. Biol. **3**, 191 (1993).

[38] J. W. Scannell, C. Blakemore, and M. P. Young, J. Neurosci. **15**, 1463 (1995).

[39] C. C. Hilgetag, G. A. Burns, M. O'Neill, J. W. Scannell, and M. P. Young, Philos. Trans. R. Soc. Lond. B, Biol. Sci. **355**, 91 (2000).

[40] C. C. Hilgetag and M. Kaiser, Neuroinformatics **2**, 353 (2004).

[41] C. A. S. Batista, E. L. Lameu, A. M. Batista, S. R. Lopes, T. Pereira, G. Zamora-López, J. Kurths, and R. L. Viana, Phys. Rev. E **86**, 016211 (2012); E. L. Lameu, C. A. S. Batista, A. M. Batista, K. Iarosz, R. L. Viana, S. R. Lopes, and J. Kurths, Chaos **22**, 043149 (2012).

[42] D. S. Bassett and E. Bullmore, Neuroscientist **12**, 512 (2006).

[43] D. J. Watts and S. H. Strogatz, Nature (London) **393**, 409 (1998).

[44] M. E. J. Newman, J. Stat. Phys. **101**, 819 (2000).

[45] H. Yi, J. Wang, B. Deng, X. Wei, Y. K. Wond, W. L. Chan, K. M. Tsang, and Z. Yu, Chaos **21**, 013127 (2011).

[46] M. G. Rosenblum and A. S. Pikovsky, Phys. Rev. Lett. **92**, 114102 (2004).

[47] M. Rosenblum and A. Pikovsky, Phys. Rev. E **70**, 041904 (2004).

[48] M. Rosenblum, N. Tukhlina, A. Pikowsky, and L. Cimponeriu, Int. J. Bifurcat. Chaos **7**, 1989 (2006).

[49] H. Degn, A. V. Holden, and L. F. Olsen (eds.), *Chaos in Biological Systems* (Plenum, New York, 1987).

[50] L. Glass and M. C. Mackey, *From Clocks to Chaos* (Princeton University Press, Princeton, NJ, 1988).

[51] T. Elbert, W. J. Ray, Z. J. Kowalik, J. E. Skinner, K. E. Graf, and N. Birbaumer, Physiol. Rev. **74**, 1 (1994).

[52] M. W. Slutzky, P. Cvitanovic, and D. L. Mogul, Ann. Biomed. Eng. **29**, 1 (2001).

[53] H. Korn and P. Faure, C. R. Biol. **326**, 787 (2003).

[54] N. G. Hyun, K.-H. Hyun, K.-B. Hyun, J.-H. Han, K. Lee, and B.-K. Kaang, Korean J. Physiol. Pharmacol. **15**, 371 (2011).

[55] M. E. J. Newman and D. J. Watts, Phys. Rev. E **60**, 7332 (1999).

[56] A. Destexhe, Z. F. Mainen, and T. J. Sejnowski, Neural Comput. **6**, 14 (1994).

[57] Y. Kuramoto, *Chemical Oscillations, Waves and Turbulence* (Dover, New York, 2003).

[58] N. F. Rulkov, Phys. Rev. Lett. **86**, 183 (2001).

[59] N. F. Rulkov, Phys. Rev. E **65**, 041922 (2002).

[60] C. A. S. Batista, A. M. Batista, J. A. C. de Pontes, R. L. Viana, and S. R. Lopes, Phys. Rev. E **76**, 016218 (2007).

[61] J. C. A. de Pontes, R. L. Viana, S. R. Lopes, C. A. S. Batista, and A. M. Batista, Physica A **387**, 4417 (2008).

[62] R. L. Viana, A. M. Batista, C. A. S. Batista, J. C. A. de Pontes, F. A. dos S. Silva, and S. R. Lopes, Commun. Nonlinear Sci. Numer. Simulat. **17**, 2924 (2012).

[63] C. A. S. Batista, S. R. Lopes, R. L. Viana, and A. M. Batista, Neural Networks **23**, 114 (2010).